Optimization of Segmented Earth-Jovian Transfer Trajectory Based on Solar Sail

Hanyue Shen[1]

[1]X-Institute, Shenzhen, Guangdong 518083, China

Email: shenhanyueshanghai@163.com

***Abstract*— Solar Sail is a type of novel means of propulsion without working substances. Its unique properties make it a competitive candidate for deep space missions. This research establishes a planar heliocentric model of solar sail trajectory. It optimizes a segmented E-M-J gravity slingshot sequence transfer that aims for applications in Jupiter probing missions, gaining a result with a remarkable 88% remaining mass of the spacecraft, demonstrating unmatched efficiency compared to other means of propulsion. With this extendable and rapid design strategy, this research can demonstrate the superior payload efficiency of solar sails and their potential in inter-planetary mission applications combined with traditional trajectory optimization methods and maneuvers.**

Keywords—Solar Sail, Interplanetary Flight, Orbit Design, Mathematic Modeling.

Table of Contents

Table of Variables and Conventions		
Name	**Abbrev.**	**Unit**
Semimajor Axis	**a**	**km**
Eccentricity	**e**	**NA**
Orbit Radius	**r**	**km**
Semi-Latus Rectum	**p**	**km**
Eccentricity Anomaly	**E**	**rad**
True Anomaly	**f**	**rad**
Angular Momentum	**h**	$kg \cdot km^2 \cdot s^{-1}$
Gravitation Constant	μ	$km^3 s^{-2}$
Deflection Angle	δ	**rad**
Flight Path Angle	γ	**rad**
Increment Velocity	ΔV	**km/s**
Lightness Factor	β	**NA**
Pitch Angle	α	**rad**
Clock Angle	δ	**rad**
Load Factor	σ	$kg \cdot m^{-2}$
Specific Impulse	I_{sp}	**s**

Constants		
Name	**Abbrev.**	**Quantity**
Sun Grav. Constant.	μ	**132.712e9**
Mars Grav. Constant	μ_m	**42828**
Earth Orbit Velocity	V_E	**29.78**
Mars Orbit Velocity	V_M	**24.07**
Jovian Orbit Velocity	V_J	**13.06**
Earth Orbit Radius	r_E	**149.598e6**
Mars Orbit Radius	r_M	**227.956e6**

Jovian Orbit Radius	r_J	**778.279e6**
Astronomical Unit	**AU**	**149.598e6**

I. Introduction

Jupiter is the closest gas giant to Earth, as well as a target of constant exploration. Pioneer-10 was the first to arrive at Jupiter, in 1972, and return relevant images. After Voyager's flyby, NASA launched Galileo and Juno – two Jupiter orbiters. These spacecrafts use nuclear or chemical thrusters, and hence used up a significant amount of fuel during their transfer sequences despite boosts from slingshot sequences (such as EVEEJ, EVEMJ). This resulted in small payload-mass ratios, a crucial indicator especially for long-term missions.

Taking a new means of propulsion is one way to conserve fuel. Using photonic pressure – the momentum of electromagnetic field, is hence a logical consideration as it does not use any propellants, and the only energy required is electricity to turn the solar sail to designated orientations.

A. Background Information

Solar sail is first proposed by Tsiolkovsky [1], and has been put to practice on IKAROS by JAXA and LightSail-2 by Planetary Society. In applications and in theory, designs of Luna, Mars [2][3], and other probing trajectories as well as H-reversal trajectory [4] and asteroid flyby missions have proven the significance of solar sails in deep space exploration [4], gaining more weight allocated to effective payload despite requiring a comparatively longer transfer time compared to traditional impulse engines.

Through literature review, it has been concluded that except for periodic heliocentric and cislunar orbits, few solar sail missions are designed for orbit insertion of an outer planet, while these missions are typically designed with a single segment, optimized by pseudo-spectral methods.

In this research, instead of a single segment, the optimization is carried out with multiple segments with changing control strategies, while including the effect of a Mars gravity assist flyby, which is intended to further boost the payload efficiency, providing insight to complicated and composite mission design with solar sails.

B. Global Mission Settings

In order for direct comparison to indicate the improvements of utilizing solar sails, the mission requirements will be set to that given in Interplanetary Flight Trajectory: Theory and Application [6]. The flight requires the spacecraft to enter a cis-Jovian orbit of $5R_J \times 10R_J$, where $R_J = 71492$ km is the mean volumetric radius of Jupiter. The book describes a spacecraft with initial mass 5000 kg and equipped with a chemical thruster of 450 s impulse. The initial mass is set to the same value, while the same chemical thruster is considered for arrival braking in this research.

The launch energy of the rocket is set to $0\ \mathrm{km^2 s^{-3}}$ (in the book, three solutions are given with launch energy values of over 10 [6]), and the solar sail solution is compared to three other solutions with transfer sequences and small, continuous thrust from chemical thrusters. This comparison allows the evaluation of solar sails compared to similar types of propulsion strategies, rather than drastically different strategies such as chemical impulse. The mission termination requirement is a rendezvous with Jupiter with relative velocity $0\ \mathrm{km \cdot s^{-1}}$ – any remaining velocity will be compensated with chemical thrust.

The basic material properties of the solar sail is based on existing research and assertions, taking 0.90 [7] for reflection constant and 1.2 gm^{-2} [8] for the sail surface density.

II. Hypotheses

For the sake of calculation, a few simplifications are made to the dynamics model of the system according to conventions in astronautical researches.

- Assume that planetary bodies are perfect, even spheres orbiting the sun on circular, coplanar orbits with their mean orbital radius as the radius of the circles. This sets the clock angle to $\frac{\pi}{2}$.
- The atmospheric drag of the planets is neglected, and assume that the gravitation of a body will affect the spacecraft if and only if the spacecraft is within its Hill's Sphere. Perturbation effects are hence neglected.
- The photonic pression received by the spacecraft comes only from the sun, and eclipses are neglected.
- When the spacecraft enters the Hill's Sphere, it is assumed to enter at an arbitrary point on the sphere. This is because the sphere is so small on an astronomical scale that it will, in reality, be corrected in real-time operations.
- Assume the solar sail reacts instantly to control commands.
- Assume that the propulsion efficiency of the solar sail is 100% and does not degrade [12] over time due to radiation and other effects.
- Only consider prograde transfer trajectories for energy efficiency.

With these assumptions, the dynamic model of the solar sail can be established.

III. Model Establishment

The movement of the solar sail through the interplanetary space is crucial for the solution of the problem, as well as the calculations for the assist flights and coasting ignitions.

A. Modeling the Spacecraft

In the designated condition, the spacecraft carries two sets of propulsion systems – chemical thruster and the solar sail. The chemical thruster follows the Tsiolkovsky's equation, giving that:

$$M_f = M_i \cdot \exp\left(-\frac{\Delta \mathrm{V}}{I_{sp} \cdot g}\right) \quad (1),$$

where g is the gravitational acceleration 0.0098 $\mathrm{km} \cdot \mathrm{s}^{-2}$.

Define that the 'effective payload' refers to the remaining mass of the spacecraft deducted by the mass of the solar sail. This gives a direct means of comparing whether allocating the amount of mass to solar sails is more efficient than allocating to chemical thruster propulsion.

Given that the electromagnetic radiation strength reduces in proportion to the inverse square of distance, the photonic pressure experienced at 1 AU is first given by [9]:

$$P_0 \approx 4.56\left(1 + C_{rf}\right) = 8.664\ \mu\text{Pa} \quad (2)$$

The exact deduction for the electromagnetic forces from the solar radiation flux can be found in Solar Sailing: Technology, Dynamics, and Mission Applications [10]. It will not be expanded here. Now the photonic pressure at all distances can be found.

$$P(r) = \frac{P_0}{r^2} \cdot AU^2.$$

Now, using given formulae for the solar sail, the physical properties of the spacecraft can be determined.

$$\sigma = \frac{1.53\left(1 + C_{rf}\right)}{2000\beta},$$

$$A_{sail} = \frac{5000kg}{\sigma},$$

$$M_{sail} = \rho A_{sail}.$$

For the derivation of these quantities, it can be observed that given the material properties and total weight of the spacecraft, the lightness factor will be able to correspond to unique solar sail area values. Hence, during the process of optimization for the solution, taking lightness factor as a fundamental variable is logical.

Using the above calculations about solar sail, the acceleration of the solar sail can be derived.

Recall that a generic representation of acceleration can be given by

$$a = \frac{F}{M} = \frac{P \cdot A}{M},$$

and take into consideration the pitch angle, which represents the deflection of the solar sail orientation from the radial direction:

$$\boldsymbol{a}(r, \alpha.\boldsymbol{n}) = \frac{P \cdot \cos^2(\alpha)}{\sigma}\boldsymbol{n} = \frac{\beta\mu}{r^2}\cos^2(\alpha)\boldsymbol{n}. \quad (3)$$

Note that the solar radiation force always acts normal to the sail orientation and away from the sun.

B. Heliocentric Vector Model

Adding the force contributed by the solar sail to the original two-body model will obtain the basic vector equation for the movement of the solar sail around the sun.

$$\frac{d^2\boldsymbol{r}}{dt^2} + \frac{\mu}{r^3}\boldsymbol{r} = \frac{\beta\mu}{r^2}\cos^2(\alpha)\boldsymbol{n}. \quad (4)$$

The pitch angle can take any values between $-\frac{\pi}{2}$ to $\frac{\pi}{2}$, while control strategies often tend to take a narrower range.

If the pitch angle takes its boundary values, the solar sail will be facing 90 degrees away from the sun and no propulsion will be gained, hence the equation will reduce to the original two-body equation.

Another special case is when the solar sail directly faces the sun, with a pitch angle of exactly 0 degrees. In this case, the equation can be organized into:

$$\frac{d^2\boldsymbol{r}}{dt^2} + \frac{\mu(1-\beta)}{r^3}\boldsymbol{r} = 0.$$

Since the solar radiation pressure force is proportional to the gravitation in this case, it equivalently allows the spacecraft to operate at orbits with a smaller effective gravitation constant.

Prior researches indicate that for some other special angles, the solar sail operates on a logarithmic spiral trajectory.

With the vector model established, the planar model must be transformed into a scalar equation for further operations.

C. The Cartesian Form

The Cartesian model maps the trajectory onto a plane with rectangular axis. It is utilized in the propagation of the model as it is easily compatible with existing numerical integrators.

The model used also derives some significant two-body orbital elements in order for calculation and the determination of the pitch angle, which uses control strategies dependent on orbital elements and/or time.

$$r = \sqrt{x^2 + y^2},$$

$$p = \frac{h^2}{\mu} = \frac{1}{\mu}\left(x\frac{dy}{dt} - y\frac{dx}{dt}\right)^2,$$

$$a = \left(\frac{2}{r} - \frac{\left(\frac{dx}{dt}\right)^2 + \left(\frac{dy}{dt}\right)^2}{\mu}\right)^{-1},$$

$$e = \sqrt{1 - \frac{p}{a}},$$

$$f = \cos^{-1}\left(\frac{p}{er} - \frac{1}{e}\right),$$

$$\frac{d^2x}{dt^2} = -\frac{\mu}{r^3}x + x\frac{\beta\mu}{r^3}\cos^3(\alpha) - y\frac{\beta\mu}{r^3}\cos(\alpha)\sin(\alpha), \text{(5A)}$$

$$\frac{d^2y}{dt^2} = -\frac{\mu}{r^3}y + y\frac{\beta\mu}{r^3}\cos^3(\alpha) + x\frac{\beta\mu}{r^3}\cos(\alpha)\sin(\alpha), \text{(5B)}$$

and the pitch angle will be coupled to the other quantities as given by a function of the semimajor axis, eccentricity, and true anomaly.

D. The Gauss-Lagrange Form and Control Strategies

The Gauss-Lagrange equations of motion expresses the movement of the satellite (in this case the spacecraft, regarded as a point mass) in terms of the derivatives of its six orbital elements.

The equations of motion can be view in two parts – the two-body gravitational model and a perturbation force [11]. In the case of the solar sail, we can regard the propulsion of the solar sail as a varying perturbation and integrate it with the original equation.

Under a planar scenario, the equations of concern are:

$$\frac{da}{dt} = \frac{2}{n\sqrt{1-e^2}}[f_r e\sin(f) + f_t + f_t e\cos(f)], \text{(6A)}$$

$$\frac{1}{2}\frac{de^2}{dt} = \frac{e\sqrt{1-e^2}}{na}[f_r\sin(f) + f_t\cos(f) + f_t\cos(E)], \text{(6B)}$$

$$\frac{dr_A}{dt} = (1+e)\frac{da}{dt} + a\frac{de}{dt}, \text{(6C)}$$

$$\frac{dr_P}{dt} = (1-e)\frac{da}{dt} + a\frac{de}{dt}, \text{(6D)}$$

$$n = \left(\frac{\mu}{a^3}\right)^{\frac{1}{2}}.$$

Simplify the sets of equations using conventions of the two-body motion and rearrange the equations as follows.

$$\frac{da}{dt} = \frac{2a^2}{h} \cdot \begin{bmatrix} e\sin f \\ 1 + e\cos f \end{bmatrix} \cdot \begin{bmatrix} f_r \\ f_t \end{bmatrix}, \text{(7A)}$$

$$\frac{de}{dt} = \frac{1}{h} \cdot \begin{bmatrix} p\sin f \\ er + (p+r)\cos f \end{bmatrix} \cdot \begin{bmatrix} f_r \\ f_t \end{bmatrix}, \text{(7B)}$$

$$\frac{dr_A}{dt} = \begin{bmatrix} \frac{2a^2(1+e)}{h} e\sin f + \frac{a}{h} p\sin f \\ \frac{2a^2(1+e)}{h}(1+e\cos f) + \frac{a}{h}(er + (p+r)\cos f) \end{bmatrix} \cdot \begin{bmatrix} f_r \\ f_t \end{bmatrix} \text{(7C)}$$

$$\frac{dr_P}{dt} = \begin{bmatrix} \frac{2a^2(1-e)}{h} e\sin f + \frac{a}{h} p\sin f \\ \frac{2a^2(1-e)}{h}(1+e\cos f) + \frac{a}{h}(er + (p+r)\cos f) \end{bmatrix} \cdot \begin{bmatrix} f_r \\ f_t \end{bmatrix} \text{(7D)}$$

Notice that now the change rates of the orbital elements are expressed in terms of the current orbital elements and the solar sail force components (which is in essence determined by the lightness factor and pitch angle).

When the two vectors are orthogonal, the change rate of the orbital elements is zeroed; conversely, when the two vectors are colinear, the magnitude of the change rate is maximized. This is the 'local optimal' control scheme.

Generalize the Gauss-Lagrange equations in form:

$$\frac{d\eta}{dt} = \begin{bmatrix} \lambda_1 \\ \lambda_2 \end{bmatrix} \cdot \begin{bmatrix} f_r \\ f_t \end{bmatrix}.$$

Generically, if we desire to maximize the change rate of the certain orbital element η, it is desired that the perturbation force follows the relation

$$\alpha_f = \tan^{-1}\left(\pm\frac{\lambda_1}{\lambda_2}\right). \text{(8)}$$

The 'ideal pitch angle' indicates the angle between the desired force orientation and the radial vector. The sign inside the arctangent function indicates whether the change rate is increasing or decreasing.

The control strategy for the fastest change in semimajor axis is hence:

$$\alpha_f = \tan^{-1}\left(\pm\frac{p}{re\sin f}\right).$$

And the control strategy for the fastest change in eccentricity is

$$\alpha_f = \tan^{-1}\left(\pm\frac{re + (p+r)\cos f}{p\sin f}\right).$$

When rising the orbit of the solar sail, the semimajor axis change is typically preferred to be maximized. Meanwhile, for coasting orbit, using the fastest change in eccentricity can be considered. Since eccentricity cannot be negative, taking the negative value for the strategy will place the spacecraft to a circular orbit in the fastest way.

Knowing that the force provided by the solar sail is only away from the sun, it is logical to infer that even though the optimal force orientation can be found, the solar sail might not be able to provide a force exactly in that direction.

This limitation indicates the requirement to maximize a certain component of the propulsion of solar sail.

The force of the solar sail is given by

$$\boldsymbol{F_{srp}} = PA_{sail}\cos^2(\alpha)\cdot \boldsymbol{n}.$$

And the component of propulsion along any arbitrary given orientation $\boldsymbol{k}$ can be represented by

$$\boldsymbol{F_k} = \boldsymbol{F_{srp}}\cdot \boldsymbol{k}.$$

Knowing that the 'given orientation' shall be the desired vector designated by the control strategy, the component can be rewritten in terms of the 'ideal pitch angle'.

$$F_k = PA_{sail}\cos^2\alpha\left(\cos\alpha\cos\alpha_f + \sin\alpha\sin\alpha_f\right).$$

To maximize the value, set

$$\frac{\delta F_k}{\delta\alpha} = 0;\ 2\sin\alpha\cos(\alpha-\alpha_f) + \cos\alpha\sin\left(\alpha-\alpha_f\right) = 0.$$

Solving the equation gives the pitch angle control in terms of the ideal pitch angle:

$$\alpha = \tan^{-1}\left(\frac{\sqrt{9+8\tan^2\alpha_f}-3}{4\tan\alpha_f}\right). \quad (9)$$

Now, for each control strategy, the control function for the pitch angle will be given by calculating the vector orientation of the desired force, then maximizing the solar sail's output in that direction [5].

E. The ODE Integrator

In addressing this problem, we employed the Runge-Kutta 4-5th order algorithm, also known as the Dormand-Prince method, which is widely utilized for numerically solving ordinary differential equations (ODEs).

Firstly, the Runge-Kutta 4-5th order algorithm exhibits outstanding numerical stability, making it applicable to various types of differential equation problems. The algorithm is characterized by its adaptive step-size control, a crucial aspect of its remarkable performance in practical problem-solving. Adaptive step-size control implies that the algorithm dynamically adjusts the step size based on the error estimate calculated at each iteration. When greater accuracy is required, the algorithm reduces the step size to approach the solution more finely. Conversely, when the problem is relatively simple or the solution is sufficiently close to the true solution, the algorithm increases the step size to enhance computational efficiency. This adaptability enables the Runge-Kutta 4-5th order algorithm to maintain high precision while better accommodating the characteristics of different problems. Furthermore, the Runge-Kutta 4-5th order algorithm generally demonstrates favorable numerical stability across various types of differential equations. Numerical stability refers to the algorithm's ability to avoid numerical instability or divergence during the iteration process. This quality positions the Runge-Kutta 4-5th order algorithm as a reliable tool, particularly suitable for solving ordinary differential equations.

F. Rendezvous with Planets

An important trait of this designed mission is the integration of a Mars gravity slingshot assist flyby. The excess velocity upon reaching Jupiter is also needed for the evaluation of the optimization.

First consider the spacecraft reaching Mars. By definition, the excess velocity can be determined by

$$V_\infty = \sqrt{V_-^2 - V_M^2},$$

Note that due to the symmetry of the hyperbolic trajectory, the magnitudes of the incoming and departure excess velocities under Martian frame are equal, but with a deflection angle, which is the eventual cause of the slingshot effect, changing the heliocentric velocity. Hence the orbital elements of the hyperbolic trajectory can be solved for given the excess velocity.

$$a = -\frac{\mu_M}{V_\infty^2},$$

$$e = 1 - \frac{r_P}{a}.$$

Note that here, the perigee orbital radius under the Martian frame is undetermined. This is because, reviewing the hypothesis section, the incoming location of the spacecraft is arbitrary, and hence even though the semimajor axis is certain due to the certainty of the orbital energy, the eccentricity is very much to be determined. As later process will discuss, however, this value will be set to 100 km after calculation.

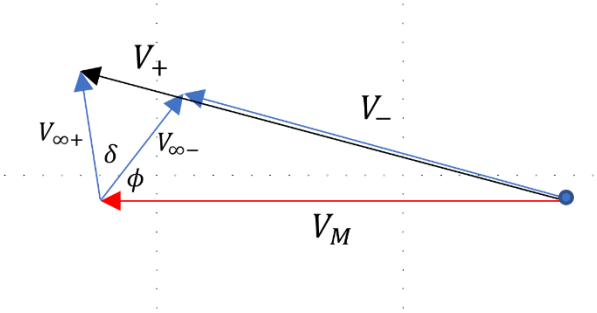

Figure 1. Vector quantity relationships of the Martian flyby.

To correctly output resultant angles, the relative angle of the incoming velocity under Martian frame must be found. Recall that it has been assumed that planets orbit on circular trajectories, and hence the angle between the Martian velocity vector and the incoming heliocentric frame velocity will exactly be the heliocentric flight path angle, and using the law of sines we have:

$$\frac{\sin\phi}{\sin\gamma_-} = \frac{V_-}{V_\infty}.$$

By definition, the deflection angle is given by

$$\delta = 2\sin^{-1} e^{-1}.$$

And hence, calculate the heliocentric departure velocity magnitude and flight path angle using the law of cosine and law of sine.

$$V_+ = \sqrt{V_\infty^2 + V_M^2 - 2V_\infty V_M \cos(\delta + \phi)}, \text{(10A)}$$

$$\frac{\sin\gamma_+}{\sin(\delta+\phi)} = \frac{V_\infty}{V_+}. \text{(10B)}$$

Using this set of calculations, we are able to determine the motion of the spacecraft after its Martian flyby given its initial state.

The benefit of passing Mars is a considerable boost in the orbital velocity of the spacecraft, and hence decreasing the mission time required.

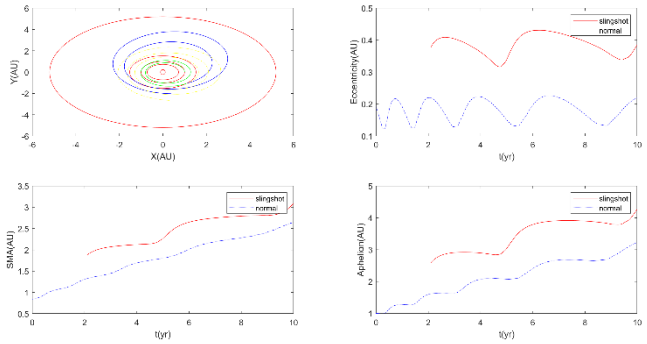

Figure 2. Comparison between a gravity assist (red) and without gravity assist (blue).

As shown by the example, for a solar sail operating under a constant control strategy, passing Mars for a slingshot effect increases semimajor axis, aphelion radius, as well as eccentricity, flinging the spacecraft off to a higher heliocentric orbit.

The arrival of Jupiter involves orbital insertion, which is the transfer from a hyperbolic trajectory to a given elliptic orbit. The impulse needed is given by

$$\Delta V = \sqrt{\frac{2\mu_J}{r_P} + V_\infty^2} - \sqrt{\frac{2\mu_J}{r_P} - \frac{\mu_J}{a}}. \quad (11)$$

Given the semimajor axis (the average of the perigee and apogee radius) and the perigee radius, the impulse can be calculated and hence the fuel used can be determined.

From the expression, it can be determined that given the targeted orbit, minimizing the impulse indicates minimizing the excess velocity. Hence, to conserve the chemical fuel, the spacecraft must minimize its relative speed when approaching Jupiter.

G. Target Function

The target function is the quantitative evaluation for the optimization process. In this scenario, the effective payload is aimed to be optimized. Hence, the target function can be generically given by

$$\text{minimize } \Delta Mass = M_i \cdot \left(1 - \exp\left(-\frac{\Sigma \Delta V}{I_{sp} \cdot g}\right)\right) + M_{sail}, \quad (12)$$

With the target function, the sequence of design can now be carried out.

IV. Simulation Results and Discussions

In this section, the structure of the mathematical model written in Matlab is explained and crucial data of the optimization process is shown.

A. Program Structure

Aside from the main control program, the simulation is consisted of five programs: the integrator, the flyby calculator, the rendezvous calculator, the transition time optimizer, and the strategy optimizer.

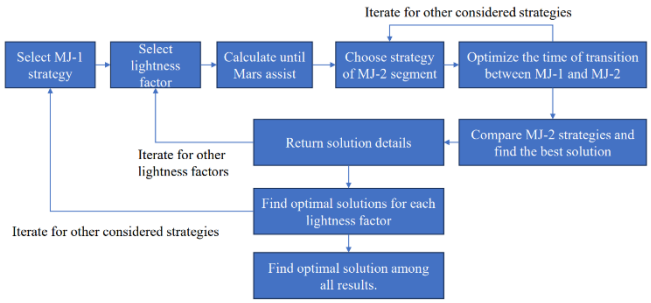

Figure 3. Simulation flowchart.

To use the set of simulations, due to the complexity of the calculation and the amount of time required for each iteration, the researchers input the lightness factor as a discrete variable ranging from 0.025 to 2, inclusive, varying by steps of 0.025.

B. Settings before Optimization

There are three segments of trajectory considered: EM (Earth-Mars Transfer), MJ-1 (Mars-Jupiter Interplanetary Transfer), and MJ-2 (Mars-Jupiter Coasting Transfer).

The five types of strategies considered for the MJ-1 segment are SMA+ (fastest semimajor axis increase), ECC+ (fastest eccentricity increase), ECC- (fastest eccentricity decrease), PER+ (fastest perihelion increase), APO+ (fastest aphelion increase). The five types of strategies considered for the MJ-2 segment are: SMA+, SMA- (fastest semimajor axis decrease), ECC-, PER+, APO+. Note that ECC+ strategy is not considered for the second segment, for increasing the eccentricity is not beneficial for the reduction of relative velocity in rendezvous, and hence should be used in raising the cis-solar orbit, not the coasting segment. We set maximum time for both segments to 15 years in order to limit the iteration convergence.

The EM segment considers two strategies only: SMA+ and APO+. This is because the first segment is not an arrival segment – simply a flyby. Hence, the spacecraft should aim to meet with Mars as soon as possible.

Hence, before carrying out the process of optimization, the EM segment as well as the perigee under Martian frame must be determined.

Let the lightness factor be 0.05, calculate the optimized program with the EM segment set to SMA+ strategy.

Table 1. Effect of varying Mars perigee.

PER (km)	MJ-1	MJ-2	Total Time (yrs)	Payload (kg)
100	SMA+	PER+	20.05	3352
150	SMA+	SMA+	20.08	3319
200	SMA+	SMA+	20.02	3303

Through this comparison, it is indicated that while other factors are kept the same, allowing the spacecraft to flyby at a lower altitude result in a larger effective payload in the end, with almost no effect to the total time taken for the mission. However, an

excessively close flyby will cause the spacecraft to be trapped by the atmosphere of the planet, and hence the perigee radius of **100 km** is eventually chosen.

Using simple trigonometric deduction, we can derive that lowering the perihelion altitude allows the spacecraft to gain a larger heliocentric velocity when departing from Mars. Hence, we can infer that **departing at a larger velocity and with a larger deflection angle from Mars will benefit the eventual mission results**.

Comparing the two strategies for the EM sequence, the SMA+ strategy gains a 3.0019 km/s acceleration through passing Mars, while APO+ gains 3.4878 km/s. Meanwhile, the APO+ strategy gives higher heliocentric orbital eccentricity than SMA+ while their orbital energy levels are similar. Additionally, the APO+ sequence also takes a shorter transfer duration. In this case, the APO+ strategy is chosen for the EM segment.

And now we run the integrator program in order to plot and demonstrate orbital characteristics of the different control strategies involved. The intersections with Martian orbit are labelled by blue circles and the optimal transition location by red asterisk.

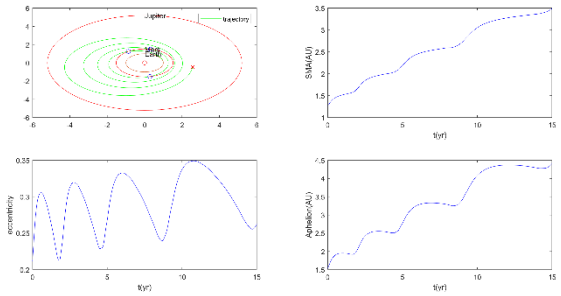

Figure 4. SMA+ Strategy.

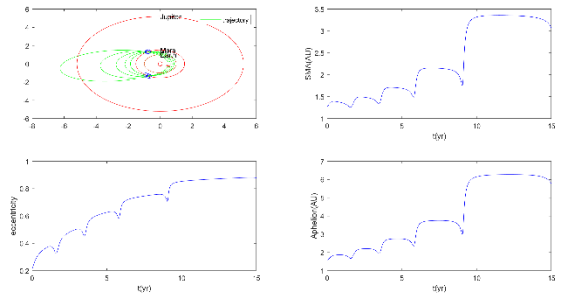

Figure 5. ECC+ Strategy.

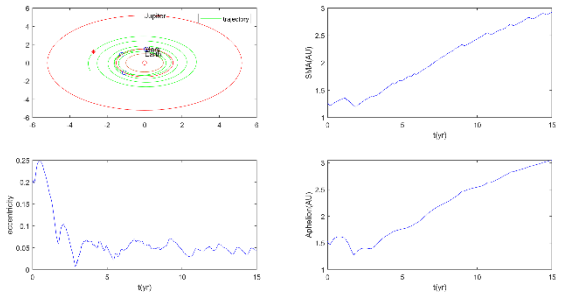

Figure 6. ECC- Strategy.

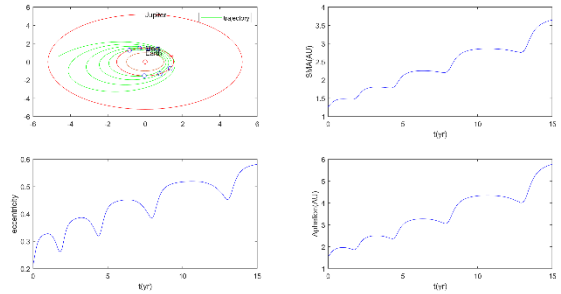

Figure 7. APO+ Strategy.

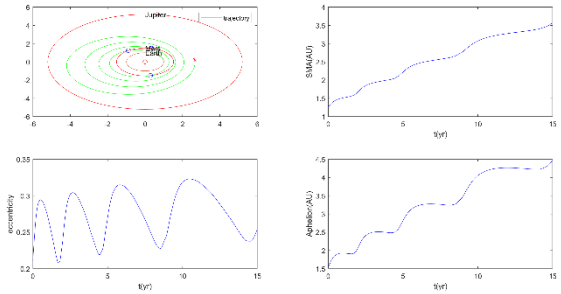

Figure 8. PER+ Strategy.

This gives an overview of the orbital properties of the local optimal control strategies, with their heliocentric trajectory, NA change, APO change, and ECC change plotted.

C. Simulation Results

After preliminary settings have been done, simulations are carried out according to the workflow described above.

An exemplary output of the program is shown.

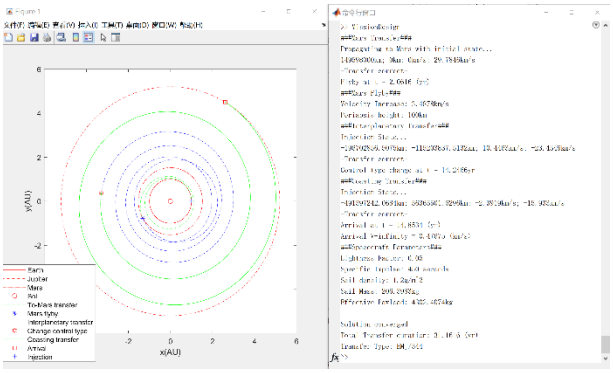

Figure 9. Exemplary output GUI.

The main program prints the calculated data by sections. For each section, the program prints the initial state of motion of the spacecraft for validation purposes. It also returns crucial end-of-stage data in order for evaluation and comparison.

The full trajectory is also plotted and labeled on a heliocentric plot for visual demonstration.

The following table lists all data from simulated calculations ran.

Table 2. Simulated datasets.

MJ-1	**MJ-2**	$\boldsymbol{\beta}$	**T (yr)**	**ΔV(km/s)**	**M_f(kg)**	**$T_{transition}$**
SMA+	PER+	0.050	20.05	1.61	3352	12.19
SMA+	ECC-	0.075	18.66	1.97	3031	11.37
SMA+	**ECC-**	**0.100**	**20.66**	**0.25**	**4400**	**5.07**
SMA+	ECC-	0.125	13.51	1.89	2980	0.27
SMA+	ECC-	0.150	10.36	1.67	3071	4.66
SMA+	ECC-	0.175	11.15	1.76	2949	0.14
ECC+	PER+	0.050	17.60	2.67	2637	1.37
ECC+	ECC-	0.075	9.74	3.10	2348	0.41
ECC+	ECC-	0.100	16.12	1.58	3257	0.55
ECC+	ECC-	0.125	14.60	1.20	3479	1.23
ECC+	ECC-	0.150	13.00	1.10	3491	0.82
ECC+	**ECC-**	**0.175**	**16.20**	**0.92**	**3572**	**2.74**
ECC+	ECC-	0.200	15.29	0.95	3475	2.33
APO+	PER+	0.050	19.05	2.05	3030	2.33
APO+	PER+	0.075	10.06	2.83	2495	0.27
APO+	ECC-	0.100	17.59	1.04	3681	2.60
APO+	ECC-	0.125	28.07	0.88	3739	12.60

APO+	**ECC-**	**0.150**	**16.80**	**0.33**	**4164**	**3.29**
APO+	ECC-	0.175	14.80	0.65	3792	1.10
ECC-	ECC-	0.050	31.16	0.48	4333	NA
ECC-	PER+	0.075	22.31	0.73	4015	6.16
ECC-	PER+	0.100	28.30	0.45	4208	13.42
ECC-	**APO+**	**0.125**	**22.73**	**0.36**	**4212**	**13.70**
ECC-	PER+	0.150	13.08	0.38	4116	4.38
ECC-	SMA+	0.175	13.17	0.59	3850	6.85
PER+	APO+	0.050	19.61	1.98	3083	12.88
PER+	ECC-	0.075	18.5	1.88	3098	10.96
PER+	**ECC-**	**0.100**	**16.3**	**0.56**	**4102**	**1.64**
PER+	ECC-	0.125	18.18	1.63	3159	8.22

In the sets of data, the five local optimal values for each control strategies of the first segment are stressed black. Since minimizing the used fuel – maximizing the remaining weight is the optimization target, the 4400 kg solution is accepted.

D. Detailed Solution

The section presents the final solution and its detailed mission data.

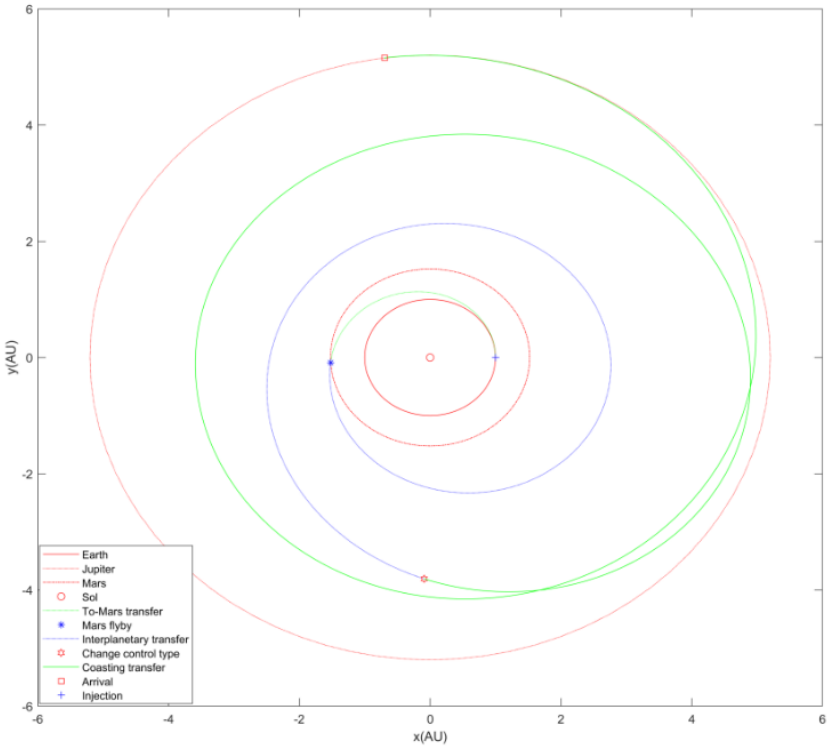

Figure 10. Detailed mission trajectory of the optimized solution.

The basic data of the spacecraft is given as well as parameters of each segment.

It should be noted that upon arriving at Jupiter, the spacecraft can discard its solar sail before engaging impulse engine to carry out orbit insertion. This can conserve fuel slightly.

Table 3. Important mission data.

Initial Weight	**Remain Weight**	**Sail Mass**
5000 kg	4400 kg	344 kg
Fuel Used	**Total Time**	**Sequence**
256 kg	20.66 yrs	EMJ/ASEM
EM Duration	**MJ-1 Duration**	**MJ-2 Duration**
0.67 yrs	5.07 yrs	14.92 yrs
C3	**Slingshot ΔV**	**Braking ΔV**
0 km^2s^{-3}	3.39 km/s	0.25 km/s

This completes the calculation and optimization process of the Jupiter-probing trajectory.

E. Comparison

As stated, in order to evaluate and validate the benefit of using a solar sail in interplanetary missions, the eventual mission data is compared to given sets of Jupiter missions with continuous small thrust solutions.

Compared to two existing impulse solutions which both have launch C3 larger than 10 km^2s^{-3} and arrival excess velocities larger than 5 km/s, solar sail holds an absolute advantage in terms of effective payload.

Moreover, even compared to a more novel impulse thrusting solution – nuclear impulse system with 2N maximum thrust at 2500s specific impulse [6], solar sailing is able to maintain its advantage, as shown below.

Table 4. Comparison with nuclear thrust system.

Factor	**Solar Sail**	**Nuclear 1**	**Nuclear 2**	**Nuclear 3**
Time	20.66	6.878	8.000	6.658
Remain Mass	4400	3385.48	3182.67	3105.54
Total ΔV	0.25	11.48	13.29	14.02

Despite its longer transfer duration of approximately 3 times that of traditional transfers, the solar sail, as shown by the table, is capable of around 40% increase in remaining mass even with a less advantageous working propulsion system. Hence, the comparison of eventual results indicates the undoubtable significance of solar sails in the improvement of payload capacity in deep space missions.

V. Conclusions

A. *Noteworthy Conclusions*

During this research, a complex, composite, and realistically set solar sail trajectory optimization is proposed and solved with segmented methods. It provides new calculations and insights into deep space exploration mission designing and points out a new possibility of astronautical propulsion system, gaining a final mass at 88% of the launch mass - vastly exceeding existing solutions. Using the strategy proposed, future unmanned and manned missions to far destinations can be carried out with significantly more efficiency - smaller numbers of spacecraft launches will be needed for a given amount of payload.

B. *Evaluations*

It should still be noted that this research holds several flaws that will be solved or compensated for in the future:

- Solar sail transfer time is relatively long although still within acceptable limits, a mixed propulsion plan might reduce the time taken;
- Taking more segments to optimize can potentially gain better results. Future studies can integrate this strategy on more complicated sequences or with new types of trajectories;
- Machine learning can be used to predict more accurate optimal values to mitigate having to use discrete values due to computational limits.

Despite these, the results gained in this research is consistent with modeling expectations and provides an improved solution, and hence will prove valuable to deep space mission designing and applications.

VI. References

[1] W.A.Hollerman, The Physics of Solar Sails, Nasa Faculty Membership Program, 2002.

[2] Yufei Guo, Dongzhu Feng, Xin Wang, Cong Li, Yunzhao Liu, ”The Earth-Mars Transfer Trajectory Optimization of Solar Sail Based on hp-Adaptive Pseudospectral Method”, Discrete Dynamics in Nature and Society, vol. 2018, Article ID 6916848, 14 pages, 2018. https://doi.org/10.1155/2018/6916848.

[3] https://dspace.mit.edu/bitstream/handle/1721.1/37176/27479802-MIT.pdf?sequence=2.

[4] Zeng, Xiangyuan and Vulpetti, Giovanni and Circi, Christian. (2018). Solar sail H-reversal trajectory: A review of its advances and applications. Astrodynamics. 3. 1-15. 10.1007/s42064-018-0032-y.

[5] Dachwald, Bernd and Ohndorf, Andreas and Wie, Bong. (2006). Solar Sail Trajectory Optimization for the Solar Polar Imager (SPI) Mission. 10.2514/6.2006-6177.

[6] Interplanetary Flight Trajectory: Theory and Application, ISBN:978-7-5682-6742-7 , Beijing Institute of Technology, 2019.

[7] R.Miller, Solar Sails - The math behind solar sails, 2015.

[8] http://www2.ee.ic.ac.uk/derek.low08/yr2proj/solarsails.htm.

[9] Richard Rieber, Principals of Solar Sailing.

[10] C.R.McInnes, Solar Sailing: Technology, Dynamics, and Mission Applications, Springer, 1999.

[11] JIANG Chunhua, XU Tianhe, QIAO Jing, et al. Derivation and Analysis of Singular-free Lagrangian/Gaussian Equations of Planetary Motion. Acta Geodaetica et Cartographica Sinica, 2018, 47(4): 455-464. DOI: 10.11947/j.AGCS.2018.20170082.

[12] Bernd Dachwald and Wolfgang Seboldt, Potential Solar Sail Degradation Effects on Trajectory and Attitude Control.